

<https://doi.org/10.1038/s41541-025-01177-y>

Regulatory T cells define affinity thresholds for CD8⁺ T cell tumor infiltration



Mona O. Mohsen^{1,2,3}✉, Romano Josi^{1,2,4}, Sanjana V. Marar², Anish Ghimire^{1,2}, Lan Yang^{1,2}, Pascal S. Krenger^{1,2,4}, Arnaud Solé Casaramona^{1,2,4}, Daniel E. Speiser^{2,3,5}, Simone De Brot⁶ & Martin F. Bachmann^{1,2,7}

TCR repertoires against tumors lack high-affinity TCRs and are further suppressed by Tregs. We hypothesized that Treg depletion enhances the antitumor efficacy of low-affinity T cells. Using the weak agonistic peptide A4Y derived from LCMV glycoprotein peptide p33 as a model antigen and VLPs as a vaccine platform, we tested this approach. In a separate low-affinity model, we targeted B16F10 melanoma with our multi-target vaccine. Results revealed limited *in vivo* lytic cross-reactivity between A4Y and p33 peptides, and the A4Y-vaccine alone failed to inhibit B16F10p33 tumor progression. However, combining A4Y-vaccine with Treg depletion triggered a robust immune response, characterized by increased CD8⁺ T cell infiltration, enhanced T cell functionality, and tumor-free survival. Infiltrating T cells also exhibited closer spatial proximity and heightened migration from blood vessels. Similarly, combining low-affinity vaccine with Treg depletion enhanced antitumor responses. These findings highlight the potential of Treg depletion to advance vaccination strategies targeting TAAs with low-affinity T cells.

The regulation of T cell responses is influenced by a multitude of factors, playing pivotal roles in orchestrating the immune response. Among these factors are the duration of antigenic stimulation, costimulatory signals from antigen-presenting cells (APCs)¹, and the affinity of T cell receptor (TCR) for peptide-major histocompatibility complex (pMHC)^{2–3}. T cells exhibit a spectrum of activation levels in response to pMHC ligands including the complete activation of intricate signaling pathways, cellular proliferation, secretion of cytokines, and the execution of target cell destruction such as in the case of cytotoxic CD8⁺ T cells. Low-affinity T cells have reduced binding to pMHC which results in suboptimal immune response. Nevertheless, low-affinity T cells may be able to propagate the signaling cascade, expand and differentiate during an immune response^{4,5}. Tumor-associated antigens (TAAs) are defined as molecules expressed by tumor cells that are either overexpressed, aberrantly expressed, or uniquely expressed compared to normal cells⁶. Epitopes derived from TAAs are generally recognized by the TCR with low to moderate affinity due to partial immune tolerance⁷. Accordingly, increased antigen densities may be needed to trigger full T cell activation if that is possible at all. However, despite specific recognition,

TAAs frequently fall short in effectively mediating cancer cell elimination⁸, rendering the full activation program in low-affinity T cell, an important goal in tumor immunotherapy.

Regulatory T cells (Tregs) play a pivotal role in maintaining self-tolerance. By safeguarding against autoimmune disease and immunopathology while orchestrating the immune response to potentially harmful infections, Tregs substantially contribute to immune homeostasis⁹. Over time, researchers have identified various immunosuppressive T cell populations in humans, including T_H3 cells, Type 1 Tregs, and the classical Tregs characterized by the expression of the transcription factor Forkhead Box P3 (FOXP3)¹⁰. FOXP3⁺ T cells remain the subject of intense studies. Peripheral Tregs recognize a range of self and non-self-peptides derived from pathogens or ingested food to sustain mucosal tolerance, avert allergic reactions, and suppress inflammation and tissue damage^{11,12}. There is growing evidence that peripheral Tregs in cancer suppress the antitumor immune response. For instance, in ovarian cancer patients, the proportion of peripheral Tregs was markedly elevated compared to individuals with benign tumors or healthy ovarian tissues¹³. Similar findings were made in

¹Department of Rheumatology and Immunology, Inselspital, University of Bern, Bern, Switzerland. ²Department for BioMedical Research, University of Bern, Bern, Switzerland. ³DeepVax GmbH, 8487 Rämismühle, Zürich, Switzerland. ⁴Graduate School for Cellular and Biomedical Sciences (GCB), Bern, Switzerland.

⁵Department of Oncology, Lausanne University Hospital and University of Lausanne, Lausanne, Switzerland. ⁶COMPAT, Institute of Animal Pathology, University of Bern, Bern, Switzerland. ⁷Nuffield Department of Medicine, The Henry Wellcome Building for Molecular Physiology,

The Jenner Institute, University of Oxford, Oxford, UK. ✉e-mail: mona.mohsen@unibe.ch

adenocarcinoma, colorectal, breast, pancreatic, lung, head and neck squamous cell carcinoma, and liver cancer¹⁴.

Furthermore, during high dose of LCMV infection it has been shown that chronic infection caused significant Treg expansion and upregulation of PD-1, enhancing their suppressive capacity on both CD8⁺ and CD4⁺ T cells¹⁵. The study identified the PD-1 interaction between Tregs and CD8⁺ T cells as a key mechanism for immune suppression, suggesting that PD-1 expression on Tregs contributes to immune regulation in chronic viral infection.

Here we studied the functional activity (antitumor protection, cytotoxicity, cross-reactivity, and tumor infiltration capability) to understand the interplay between low-affinity T cells and Tregs. We used the low-affinity A4Y peptide derived from LCMV as model antigen, and bacteriophage Q β -VLPs, packaged with B-type CpGs as TLR9 ligands as vaccine. Our results demonstrate a limited cross-reactivity of T cells induced by the low-affinity A4Y peptide to the original ligand p33. The low-affinity vaccine failed to protect against B16F10p33 tumor growth. We compared the antitumor efficacy of the low-affinity vaccine with and without the Treg depletion. Interestingly, the elimination of Tregs resulted in much stronger effects of the low-affinity vaccine, with enhanced antitumor activity and efficient infiltration of CD8⁺ T cells in the tumor, as well as reduced necrosis. Through deep learning (DL)-based histology assessment, we demonstrated that the distance between individual CD8⁺ T cells was significantly reduced in mice treated with Q β -A4Y combined with anti-CD25, compared to Q β -A4Y vaccination alone. Additionally, CD8⁺ T cells were able to infiltrate more deeply into the tumors and migrate further away from the blood vessels when Tregs were depleted. These findings unveil a novel effect of Tregs, namely their ability to restrain the potential of low-affinity T cells. As an additional model, we used our previously developed multi-target TAA vaccine which showed enhanced efficacy when combined with Treg depletion. Our insights pave the way for innovative therapeutic avenues that aim to harness the latent potential of low-affinity T cells for cancer immunotherapy.

Results

Limited cross-reactivity of the low-affinity A4Y peptide

A4Y of LCMV is a low-affinity ligand for TCR of P14 mice with amino acid substitution at position 4, wherein the original tyrosine (Y) was replaced with an alanine (A). Former computer modeling and experimental evidence have shown that the Y at position 4 points out of the MHC groove toward the TCR (cartoon in Fig. 1A). The binding affinity of A4Y peptide for H-2D^b MHC molecule has previously been shown to be in the range of 10⁻¹⁰ M, similar to the original p33 peptide¹⁶. To investigate possible cross-reactivity of the polyclonal T cell response in vivo, we generated vaccines using our CpG-loaded Q β -VLPs. A4Y or p33 peptide was chemically linked to Q β (hereafter Q β -A4Y or Q β -p33) using our well-established Cu-free click chemistry technique^{17–19}. Q β (1668)-VLPs (without peptide, hereafter Q β) were used as a control. Successful CpG packaging and peptide coupling were confirmed using agarose gel and SDS-PAGE, respectively (Fig. 1B, C).

To assess the in vivo induction of tetramer-specific CD8⁺ T cell response, wild-type C57BL/6 mice were vaccinated subcutaneously with a single dose of 50 μ g of either Q β -A4Y or Q β -p33 vaccines. As a control, mice were vaccinated with Q β only. The spleens of the vaccinated mice were harvested eight days later, at the peak of the immune response. To assess the frequencies of A4Y- or p33-specific T cells, tetramer staining was employed (Suppl. Fig. 1A). As anticipated, vaccination against A4Y or p33 resulted in a strong T cell response, with approximately 2–9% of the total CD8⁺ T cells being specific for the respective peptide (Fig. 1D–G for representative flow cytometry plots). Immunization with Q β alone did not activate A4Y or p33-specific T cell responses. Minimal insignificant cross-reactivity between the two T cell populations was detected by tetramers (Fig. 1H). Subsequently, we evaluated IFN- γ cytokine secretion. Notably, there was an observable secretion of IFN- γ in the groups vaccinated with Q β -A4Y or Q β -p33 when stimulated with the corresponding peptide (Fig. 1I, J and Suppl. Fig. 1B, and Fig. 1K for representative flow cytometry plots). The collective data indicate

a robust and specific immune response generated by these vaccines but limited cross-reactivity.

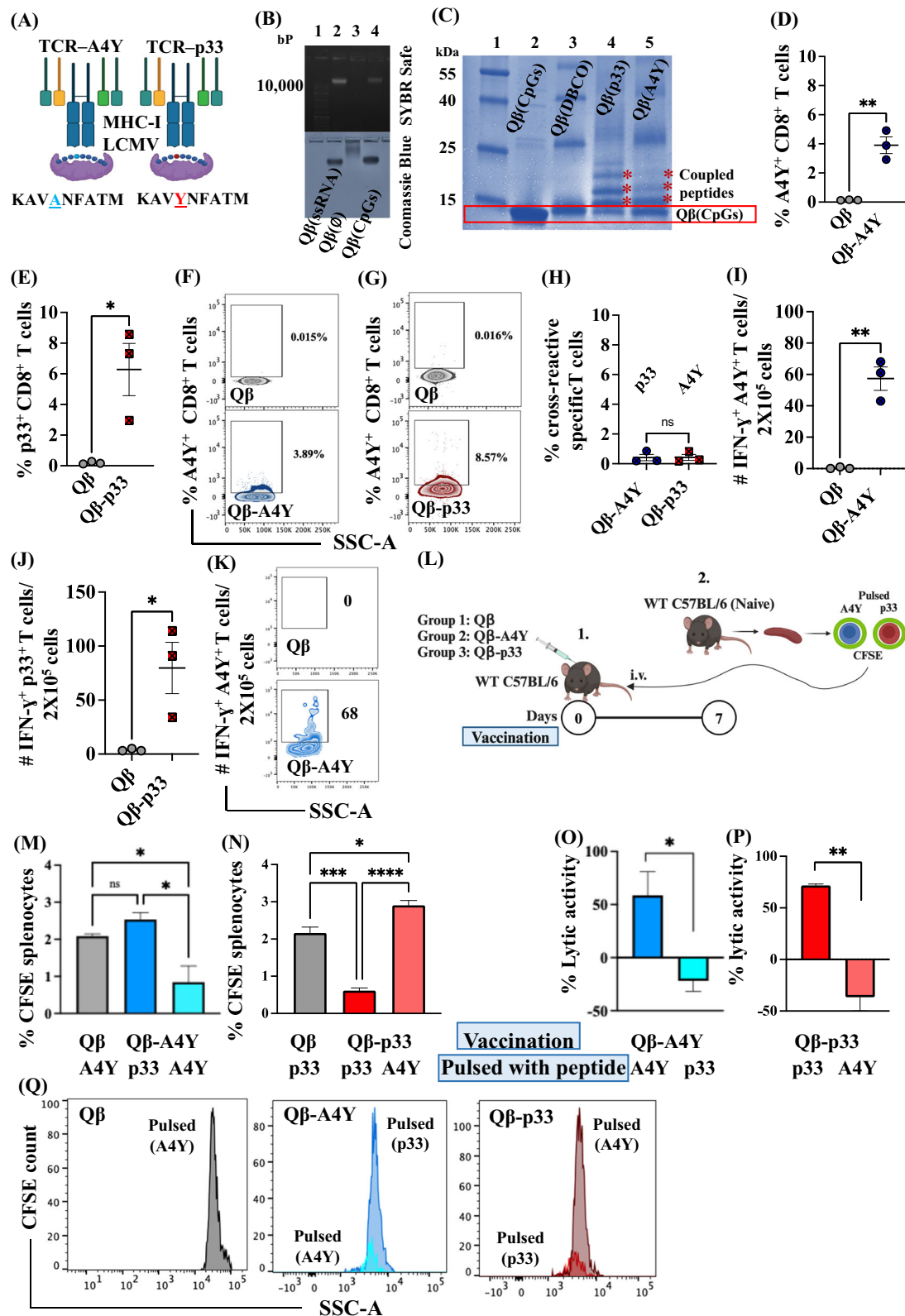
To examine the lytic activity of the induced T cells, we conducted an in vivo CFSE cytolytic assay. Wild-type C57BL/6 mice were vaccinated subcutaneously with 50 μ g of either Q β -A4Y or Q β -p33. After seven days, mice were perfused with CFSE-labelled splenocytes that had been pulsed with A4Y or p33 antigens, following the procedure illustrated in Fig. 1L. Four hours later, we performed flow cytometry to evaluate the percentage of CFSE-labeled splenocytes in each group. We observed a significant decrease in the percentage of A4Y-pulsed splenocytes in the group vaccinated with Q β -A4Y, compared to the control group vaccinated with Q β (Fig. 1M). Importantly, no reduction was observed of p33-pulsed splenocytes in Q β -A4Y vaccinated mice. In turn, mice vaccinated with Q β -p33 showed strong reduction of p33-pulsed splenocytes but not A4Y pulsed splenocytes (Fig. 1N). The lytic activity of Q β -A4Y and Q β -p33 was calculated (Fig. 1O, P). A representative histogram of CFSE percentage is displayed in Fig. 1Q. Collectively, these findings indicate limited in vivo cross-reactivity between A4Y and p33.

Low-affinity vaccine induces a systemic T cell response but fails to hinder the progression of B16F10p33 melanoma

Next, we investigated whether the low-affinity vaccine Q β -A4Y could trigger an antitumor response in wild-type C57BL/6 mice bearing B16F10 melanoma tumors transfected with p33 peptide (B16F10p33). We used our previously established and challenging-to-treat therapeutic tumor model, which consists of transplanting tumor fragments of approximately 8 mm³ in size in the flank of wild-type naïve mice^{17,20} (Fig. 2A). Therapeutic vaccination began 3 days after tumor transplantation. Over the course of 14 days, mice received 3 doses of 50 μ g of either Q β control, Q β -A4Y, or Q β -p33, with the initial dose administered on day 3 post-tumor transplantation, followed by 2 boosts on days 7 and 10. Tumors were collected for analysis on day 14 (Suppl. Fig. 1C). Vaccination with Q β -A4Y or Q β -p33 resulted in a systemic increase in A4Y- or p33-specific T cells, confirmed by blood analysis on day 11 post vaccination (Fig. 2B–D for representative flow cytometry plots). Despite the expansion of circulating CD8⁺ T cells following vaccination with either Q β -A4Y or Q β -p33, only Q β -p33 vaccine exhibited a significant ability to hinder the progression of B16F10p33 tumors ($p = 0.0009$) (Fig. 2E, F). The low-affinity Q β -A4Y vaccine did not significantly hinder melanoma progression ($p = 0.1188$) (Fig. 2E, F), although a tendency to reduced tumor size was observed. To study the capacity of the induced T cells to infiltrate the tumor, we assessed A4Y- and p33-specific CD8⁺ T cells in each tumor at the end of the experiment by flow cytometry. Our data demonstrate that both vaccines were effective in increasing T cell infiltration ($p = 0.0022$ and $p = 0.0087$, respectively) as depicted in Fig. 2G–I for representative flow cytometry, albeit vaccination with Q β -p33 was more efficient. This suggests that despite the differences in the vaccines' impact on melanoma progression, both vaccines successfully promoted the infiltration of specific CD8⁺ T cells into the tumors. Interestingly, the p33/A4Y T cell ratio was higher in tumors than in blood in A4Y-immunized mice, indicating that at least some A4Y-specific T cells also interacted with peptide p33 and were enriched in p33-expressing tumors (Fig. 2J).

Treg depletion enables in vivo lytic CD8⁺ T cell responses to Q β -A4Y vaccination

Next, we combined the low-affinity Q β -A4Y vaccination with anti-CD25 mAb treatment to deplete Tregs. In this experiment, we studied four distinct groups: Q β , Q β -A4Y, Q β -A4Y combined with Treg depletion (Q β -A4Y/Tregs depl), and Treg depletion alone as an additional control. The vaccine was administered subcutaneously while the mAb was injected intravenously as illustrated in Fig. 3A. We tested two doses of anti-CD25 mAb (10 μ g and 20 μ g) in combination with the Q β -A4Y vaccine 48 hours post- intravenous injection to ensure minimal depletion of CD4⁺ effector T cells (Suppl. Fig. 2). Both doses effectively depleted FOXP3⁺ T cells without significantly affecting the overall CD4⁺ T cell population. Based on these results, we



selected the 10 μ g dose for further experiments. We confirmed the depletion of Tregs in the blood of vaccinated mice on day 5, as we found that the CD4⁺ CD25^{hi} FOXP3⁺ T cells were nearly 100% eliminated (Fig. 3B, C). Treatment with Q β , Q β -A4Y or anti-CD25 mAb alone did not exhibit antitumor efficacy (Fig. 3D, E). Interestingly, combining the low-affinity Q β -A4Y vaccine with anti-CD25 mAb resulted in almost complete antitumor

protection when compared to the groups vaccinated with Q β , Q β -A4Y or anti-CD25 alone ($p \leq 0.0001$, $p = 0.0034$ and $p = 0.0007$ respectively) (Fig. 3D, E). Next, we assessed the density of A4Y-specific CD8⁺ T cells in the tumors across the different experimental groups. Our data showed a significant increase in the density of A4Y-specific T cells in the tumor in the group that received the low-affinity vaccine combined with Treg depletion

Fig. 1 | Limited cross-reactivity of the low-affinity A4Y peptide. **A** A cartoon illustrating antigen presentation of the low-affinity A4Y glycoprotein peptide (KAVANFATM) and p33 (KAVYNFATM). In A4Y variant, tyrosine (Y) is substituted by alanine (A) at position 4. **B** 1% agarose gel electrophoresis image, with Lane 1, DNA ladder; Lane 2, Q β (ssRNA); Lane 3, Q β (ϕ) empty; Lane 4, Q β (CpGs). ODN 1668, TLR9 was used in all experiments. The top part of the gel is stained with SYBR Safe, while the bottom part is stained with Coomassie Blue. **C** SDS-PAGE stained with Coomassie Blue, with Lane 1, protein marker; Lane 2, Q β (CpGs) at 14 kDa; and Lane 3, Q β (CpGs) derivatized with a dibenzocyclooctyne bifunctional cross-linker (DBCO), Lanes 4 and 5 show coupling to p33 or A4Y peptides respectively. Red box indicates Q β (CpGs) monomer before and after derivatization with DBCO and coupling to peptides. Black arrows indicate the coupled peptides to a

Q β monomer. **D, E** Percentage of A4Y $^{+}$ and p33 $^{+}$ cells within CD8 $^{+}$ T cells in the spleen, measured 8 days post-vaccination with Q β control, Q β -A4Y or Q β -p33. **F, G** Representative flow cytometry plots of (**D, E**). **H** Percentage of cross-reactive specific T cells. **I, J** Number of IFN- γ producing A4Y $^{+}$ and p33 $^{+}$ cells within CD8 $^{+}$ T cells in the spleen per 2×10^5 splenocytes, measured 8 days post-vaccination with Q β , Q β -A4Y or Q β -p33. **K** Representative flow cytometry plots of (**I**). **L** Experimental setup for the assessment of killing in vivo. **M, N** Percentage of CFSE labeled splenocytes, pulsed with A4Y or p33 peptide in mice vaccinated with Q β , Q β -A4Y, or Q β -p33. **O, P** Percentage of in vivo lytic activity. Please note that negative lytic activity normally occurs in this type of analysis. **Q** Histograms showing the count of CFSE-pulsed splenocytes. Statistical analysis with Student's *t*-test or one-way ANOVA. The sample size for each group was $n = 3$.

(Fig. 3F) when compared to the other groups ($p = 0.0038$, $p = 0.0121$ and $p = 0.0038$, respectively). Next, we evaluated the functional activity of TILs, which were restimulated with A4Y peptide. We observed a trend towards increased IFN- γ secretion from A4Y-specific T cells in the tumor in both groups receiving the Q β -A4Y vaccine; however, it was not statistically significant (Fig. 3G). Representative flow cytometry plots of the total number of A4Y-specific cells in the tumor across the different groups are shown in Fig. 3H. Collectively, these findings indicate that depleting Tregs effectively empowers low-affinity T cells to exert efficient tumor protection. Combining the high affinity Q β -p33 with Treg depletion did not enhance the antitumor efficacy (Suppl. Fig. 3).

Treg depletion promotes tumor-free survival mediated by specific T cells

Our promising data of combining the low-affinity Q β -A4Y vaccine with Treg depletion prompted us to investigate the ability of this combination therapy to prevent tumor relapse following the surgical resection of the primary tumor. An illustration of the experimental plan is shown in Fig. 4A. The primary tumor was resected with clear margins on day fourteen and mice were closely followed and monitored for 100 days for any sign of tumor recurrence or relapse without any additional immunization. The results showed ~83% tumor-free survival in the group that received the low-affinity Q β -A4Y vaccine combined with Treg depletion with an overall significance of $p < 0.0001$ (Fig. 4B). Importantly, tumor-free survival with Q β -A4Y/Treg depletion was significantly higher than with vaccination using Q β -A4Y alone ($p = 0.0336$) (Fig. 4B, C shows the median survival in days and the survival rate at days 49 and 100).

Next, we assessed the presence of tissue-resident memory T cells (T_{RM}) in the tissue surrounding the previously resected primary tumor (Fig. 4A) in the group that was vaccinated with Q β -A4Y/Treg depletion (as these mice were the only ones protected for 100 days). Although comparative analysis is essential and can provide additional context, it was not feasible due to survival limitations, and euthanasia of the other groups was carried out following the regulations outlined in the Swiss Animal Act. T_{RM} -specific were identified based on the expression of CD8, A4Y $^{+}$ tetramer, and the surface markers CD103²¹, CD62L and CD69. We focused on investigating the different T_{RM} subsets following vaccination with the low-affinity vaccine in the absence of Tregs in mice that survived for 100 days post tumor transplantation. We performed an unbiased and high-dimensional analysis of the acquired flow cytometry data (5 samples were concatenated for analysis from each group), focusing on A4Y tetramer and CD8, CD103, CD69, and CD62L surface markers. We employed the non-linear dimensionality reduction technique, t-distributed stochastic neighbor embedding (tSNE), followed by FlowSOM analysis to identify distinct T cell clusters (Fig. 4D). We identified five distinct T cell clusters (Pop 0–4), as visualized in the generated heatmaps (Fig. 4E). Populations 2 and 3 (3.81% and 4.28%) showed the highest expression of A4Y tetramer and CD8 marker. Population 3 further expressed αE CD103 integrin and to a lower extent the activation marker CD69; both markers are essential for identifying T_{RM} cells. Furthermore, Population 3 showed no expression of the L-selectin marker CD62L. Populations 0 and 1 exhibited no expression of A4Y

tetramer but showed variable expression of CD8 and CD62L surface markers. Population 4 had a lower expression of A4Y tetramer, CD8, and CD103 surface markers. Together, these findings establish that the depletion of Tregs, when combined with a low-affinity vaccine, can effectively elicit a durable and specific immune response, both locally and systemically, offering protection against tumor growth. Figure 4F shows representative tSNE plots for each individual marker.

Enhanced tumor infiltration by low-affinity T cells in the absence of Tregs

To gain a more comprehensive understanding of T cell localization in the tumor following treatment, we performed hematoxylin and eosin (HE) staining and immunohistochemistry (IHC) for CD8 $^{+}$ T cells. The quantification of CD8 $^{+}$ T cells was performed digitally using DL-based histology analysis. We divided the tumor tissue into several areas for simpler analysis. We assessed and quantified CD8 $^{+}$ T cells in the peritumor region and the intratumoral region (Fig. 5A). The peritumor region (Fig. 5A, area no. 1) is defined as the outermost 150 μm of the tumor tissue plus the adjacent 1 mm of surrounding tissue. The intratumoral region refers to the area in between these boundaries, as illustrated in Fig. 5A, area no. 2. Tissue areas with necrosis were excluded from CD8 analysis (Fig. 5A, area no. 3). The tumors were collected on day 14 and fixed in formaldehyde after measuring their weight in mg for the following groups: Q β , Q β -A4Y, Q β -A4Y with Treg depletion, and Treg depletion alone.

Our findings revealed a significant increase in the count of CD8 $^{+}$ T cells within the peritumoral region among mice who received the low-affinity vaccine combined with Treg depletion, as opposed to the remaining groups: Q β , Q β -A4Y or anti-CD25 mAb alone ($p = 0.0096$, $p = 0.006$ and $p = 0.0125$ respectively) (Fig. 5B). When assessing the density of infiltrating CD8 $^{+}$ T cells per tumor area mm^2 , a significant increase was observed solely in the group vaccinated with Q β -A4Y with Treg depletion compared to the control group that received Q β alone ($p = 0.0273$) (Fig. 5C). We have also assessed the extent of tumor necrosis as earlier research has suggested that tumor necrosis, is often attributed to factors like hypoxia and rapid cancer cell proliferation^{20,22}. Our results show a significant decrease in necrotic tissues when vaccinated with Q β -A4Y with Treg depletion in comparison to Q β alone or the group received the low affinity vaccine Q β -A4Y alone ($p = 0.0281$ and $p = 0.0255$ respectively) (Fig. 5D). Figure 5E shows representative images of tumor sections treated with Q β -A4Y with or without the depletion of Tregs.

Subsequently, we conducted additional analyses for the spatial distribution and distance measurement specifically investigating the low-affinity vaccine Q β -A4Y, with and without Treg depletion. We focused on measuring the distances between individual CD8 $^{+}$ T cells and the distance between an individual CD8 $^{+}$ T cell and the closest blood vessel, to assess the depth of infiltration away from blood vessels as illustrated in Fig. 5F. The tumor sections were double stained with anti-CD8 monoclonal antibody while the blood vessels were stained with the platelet endothelial cell adhesion molecule-1 (PECAM-1), CD31. Detection and quantification of CD8 $^{+}$ cells and CD31 $^{+}$ blood vessels were performed digitally using DL-based histology software (Visiopharm). We plotted the absolute distance

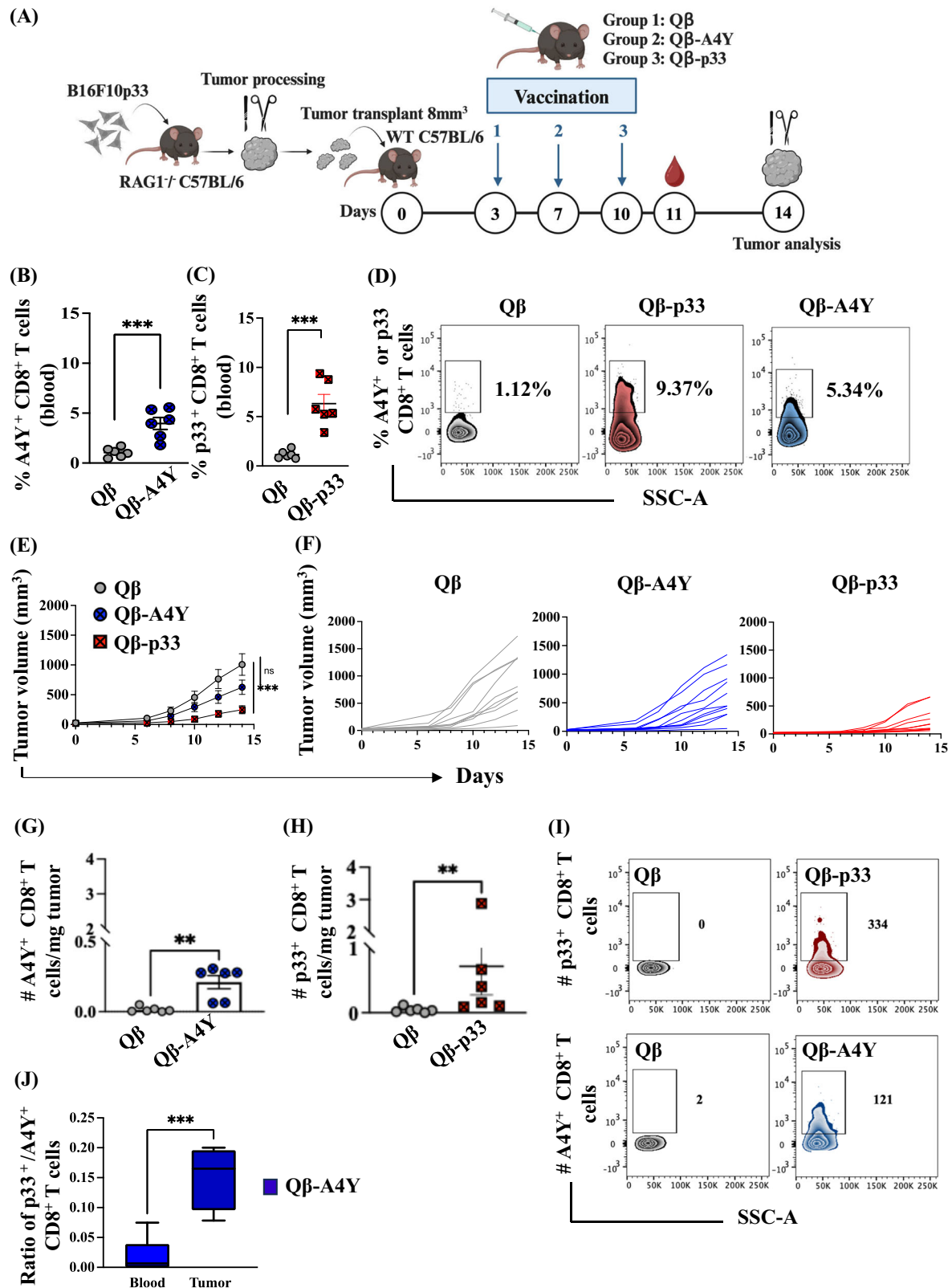


Fig. 2 | Low-affinity vaccine induces a systemic T cell response but fails to hinder the progression of B16F10p33 melanoma. **A** An illustration depicting the vaccination regimen administered following transplantation of B16F10p33 tumors. **B, C** Percentage of A4Y⁺ and p33⁺ cells within CD8⁺ T cells in the blood, measured 11 days post tumor transplantation in mice vaccinated with Q β , Q β -A4Y or Q β -p33. **D** Representative flow cytometry plots of the percentage of A4Y⁺ and p33⁺ cells within CD8⁺ T cells in the blood, measured 11 days post-vaccination. **E** Tumor

volume mm³. **F** Tumor volume mm³ of individual mice. **G, H** Densities of A4Y⁺ and p33⁺ cells within CD8⁺ T cells in the tumors on day 14. **I** Representative flow cytometry plots illustrating the total number of A4Y⁺ and p33⁺ cells within CD8⁺ T cells acquired from each tumor on day 14. **J** P33/A4Y T cell ratio in blood and tumor of mice vaccinated with Q β -A4Y. Statistical analysis with Student's *t*-test. The sample size for each group was *n* = 6.

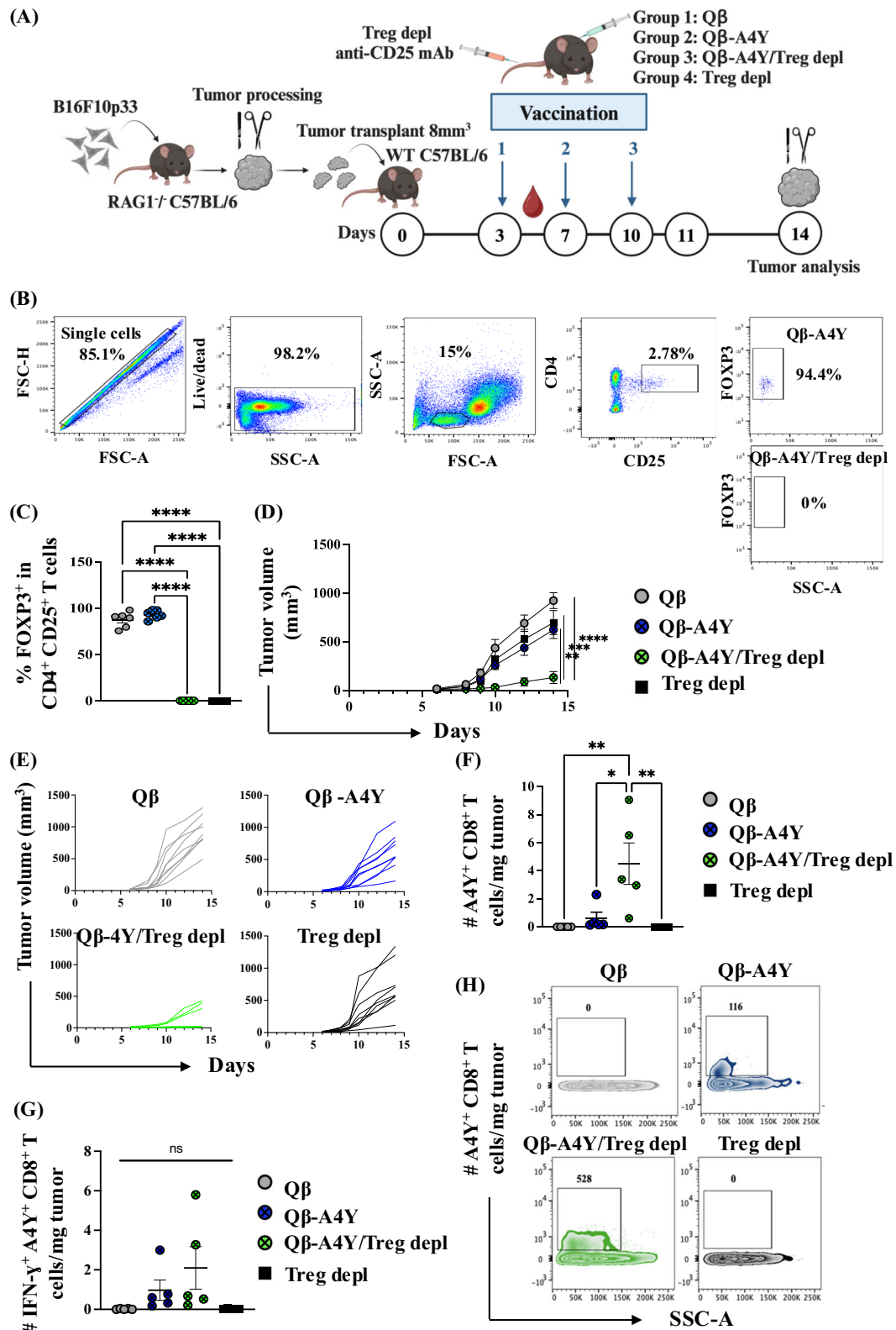
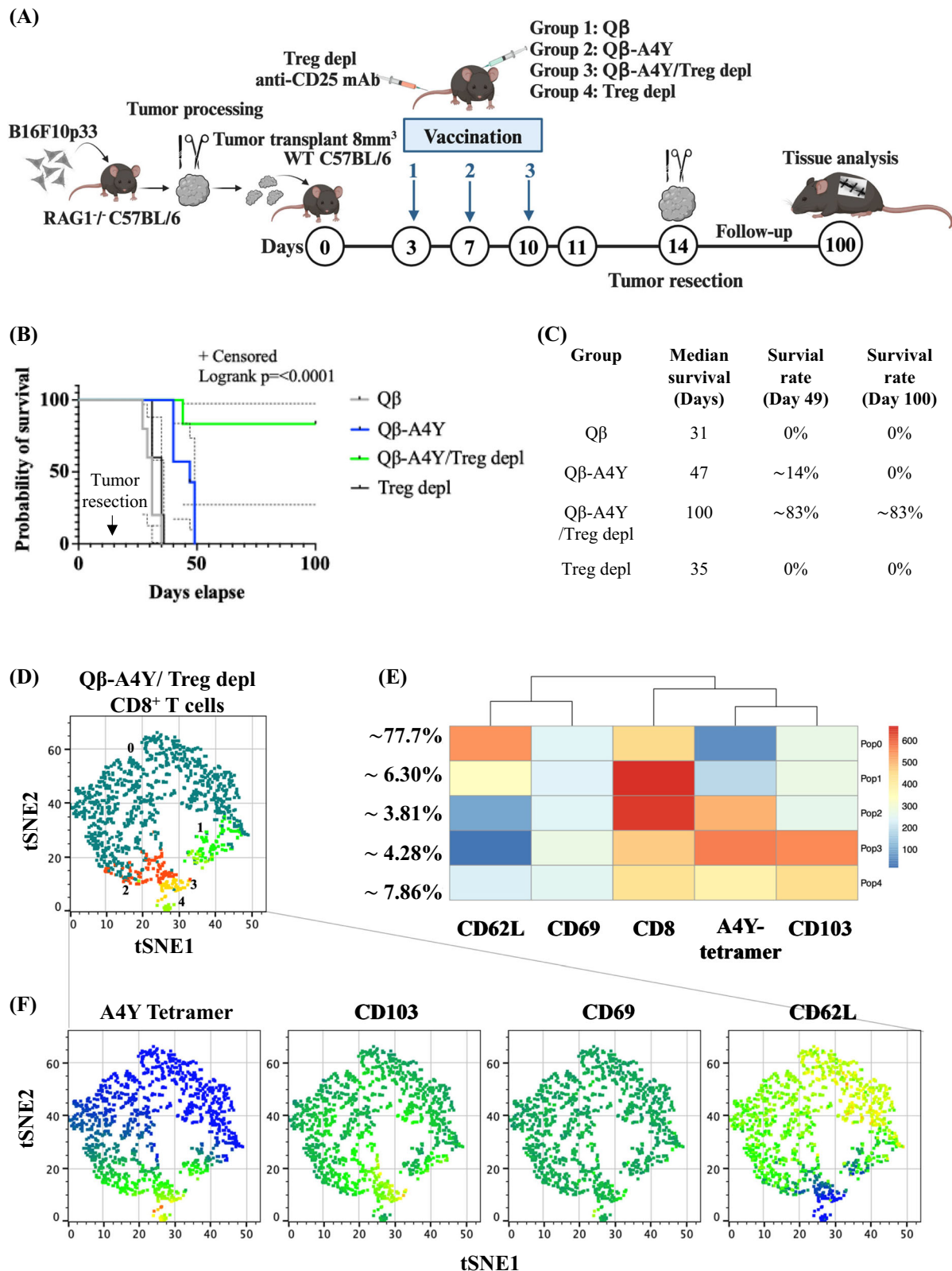


Fig. 3 | Treg depletion enables in vivo lytic CD8⁺ T cell responses to Qβ-A4Y vaccination. **A** An illustration depicting the vaccination regimen administered following transplantation of B16F10p33 tumors, combined with intravenous injection of anti-CD25 mAb for effective depletion of Tregs. Four groups were organized: Qβ, Qβ-A4Y, Qβ-A4Y/Treg depl, and Treg depl alone serving as an additional control. **B** Gating strategy of FOXP3⁺ T cells within CD4⁺ CD25⁺ T cells in the blood, measured 5 days post-vaccination and Treg depletion. **C** Percentage of

FOXP3⁺ T cells within CD4⁺ CD25⁺ T cells in the blood in the designed groups. **D** Tumor volume mm³. **E** Tumor volume mm³ of individual mice. **F** Density of A4Y⁺ cells within CD8⁺ T cells in the tumors. **G** Density of IFN-γ producing A4Y⁺ cells within the CD8⁺ T cell population in the tumor. Stimulation was conducted using the corresponding peptide. **H** Representative flow cytometry plots illustrating the total number of A4Y⁺ cells within CD8⁺ T cells acquired from each tumor. Statistical analysis with one-way ANOVA. The sample size for each group was $n = 5, 6$ or 9 .



values for both groups after setting a minimal threshold distance of 20.5 μ m between an individual CD8⁺ T cell and a blood vessel to focus on truly tumor-infiltrating T cells. Our data demonstrated a significant reduction in the proximity distance between individual CD8⁺ T cells, indicating increased clustering when combining the low-affinity vaccine Q β -A4Y with anti-CD25 mAbs ($p < 0.0001$) (Fig. 5G). Conversely, the distance between

an individual CD8⁺ T cell to the nearest blood vessels was significantly higher in this group, indicating the ability of CD8⁺ T cells to migrate deeper in the tumor in the absence of Tregs ($p < 0.0001$) (Fig. 5H). Representative IHC images are shown in Fig. 5I and Suppl. Fig. 4A. We additionally assessed the total number of CD31⁺ blood vessels in each tumor, the total number of CD31⁺ blood vessels in regions of interest (ROI) which exclude

Fig. 4 | Treg depletion promotes tumor-free survival mediated by specific T cells. **A** The experimental plan is depicted in the sketch. Primary tumors were surgically removed on day 14 under isoflurane anesthesia. Afterward, mice were monitored daily for tumor growth (recurrence). No additional vaccinations were administered after the surgical resection of the primary tumors. On day 100, the experiment was concluded and tissue surrounding the resected primary tumors was collected from tumor-free mice only. **B** Probability of tumor-free survival with 95% confidence intervals (CI) for each treatment group. Data are presented as Kaplan-Meier survival curves. **C** A table displaying the median survival (in days) and survival rates at days

49 and 100 for each treatment group. **D** Concatenated tSNE clusters for CD8⁺ T cell populations in the tissue surrounding the primary resected tumors, measured on day 100 in tumor-free mice vaccinated with Q β -A4Y/Treg depl, revealing five distinct clusters highlighted by unique colors for enhanced visualization. Markers employed include (CD8, A4Y tetramer, CD69, CD62L, and CD103), 5 concatenated samples. **E** A heatmap presenting the expression of markers within each cluster and the percentage of each population. **F** Concatenated tSNE clusters illustrating the expression of each used marker individually (data from **D**). The sample size for each group was $n = 6$ and 5.

necrosis as well as the total number of CD31⁺ blood vessels in mm². A discernible decrease was observed in tumors immunized with Q β -A4Y in combination with Treg depletion, although the difference did not reach statistical significance ($p = 0.0654$, $p = 0.0687$, and $p = 0.5756$ respectively) (Suppl. Fig. 4B–D). Thus, Tregs hinder tumor infiltration by low-affinity T cells.

Depletion of Tregs enhances induction of cross-reactive T cells

Our previous results confirmed limited cross-reactivity between A4Y and p33 in the spleen of mice vaccinated with Q β -A4Y or Q β -p33, which do not harbor a tumor (Fig. 1H). The primary objective of this experiment was to evaluate the cross-reactivity of induced A4Y- and p33-specific T cells following vaccination with the low-affinity vaccine, either alone or in combination with Treg depletion, in mice bearing the B16F10p33 tumors expressing the p33 antigen (Fig. 6A). Accordingly, B16F10p33 tumor fragments were transplanted in wild-type C57BL/6 mice which were then vaccinated subcutaneously once on day 5 with 50 μ g Q β -A4Y alone or in combination with 10 μ g anti-CD25 mAbs intravenously (Fig. 6B). A single vaccination was chosen to ensure that sufficient tumor tissue remained available for evaluating T cell cross-reactivity. Blood samples were collected 7 days following vaccination, and A4Y- and p33-specific T cells was measured. Both groups, as expected showed A4Y-specific T cell response following vaccination with Q β -A4Y (Fig. 6C, D). In addition, depleting Tregs significantly enhanced the induction of A4Y-specific T cells in the blood ($p = 0.0027$) (Fig. 6D). Interestingly, the induction of cross-reactive p33-specific T cells was significantly higher in the group received Q β -A4Y/Treg depl ($p = 0.0027$) (Fig. 6D). This is also shown in Fig. 6E, F, comparing the induced A4Y and p33-specific responses within each group separately. On day 14 post-tumor transplantation, we collected the tumors and the spleens. The group that received Q β -A4Y with Treg depletion showed reduced tumor volume when compared to Q β -A4Y alone ($p = 0.0499$), confirming previous findings (Suppl. Fig. 5). Next, we measured the density of A4Y and p33-specific T cells by flow cytometry. As shown earlier, immunization with Q β -A4Y alone resulted in infiltration of A4Y-specific T cells in the tumor, and depletion of Tregs further enhanced this infiltration as shown in Fig. 6G, H. Infiltration of cross-reactive p33-specific T cells in the tumor following vaccination with Q β -A4Y was enhanced upon depletion of Tregs (Fig. 6G, H). Figure 6I, J show a comparison of p33 and A4Y T cell densities within each group separately. We have also assessed the spleens for cross-reactive A4Y- and p33-specific T-cells. As expected, induction of A4Y-specific T cells was enhanced upon Treg depletion (Fig. 6K, L). There was a trend towards increased p33-specific T cells in the spleen of mice vaccinated with Q β -A4Y with Treg depletion, albeit not significant (Fig. 6K, L). Figure 6M, N display the percentage of A4Y and p33-specific T cells in each group separately. Collectively, these data show that depleting Tregs results in significant activation of cross-reactive T cells that recognize the p33 epitope, contributing to a broader and more effective antitumor response against B16F10p33 melanoma. Thus, elimination of Tregs not only enhances overall tumor infiltration by cross-reactive T cells but also enhances recruitment of cross-reactive T cells with high affinity for p33 and presumably low-affinity for A4Y.

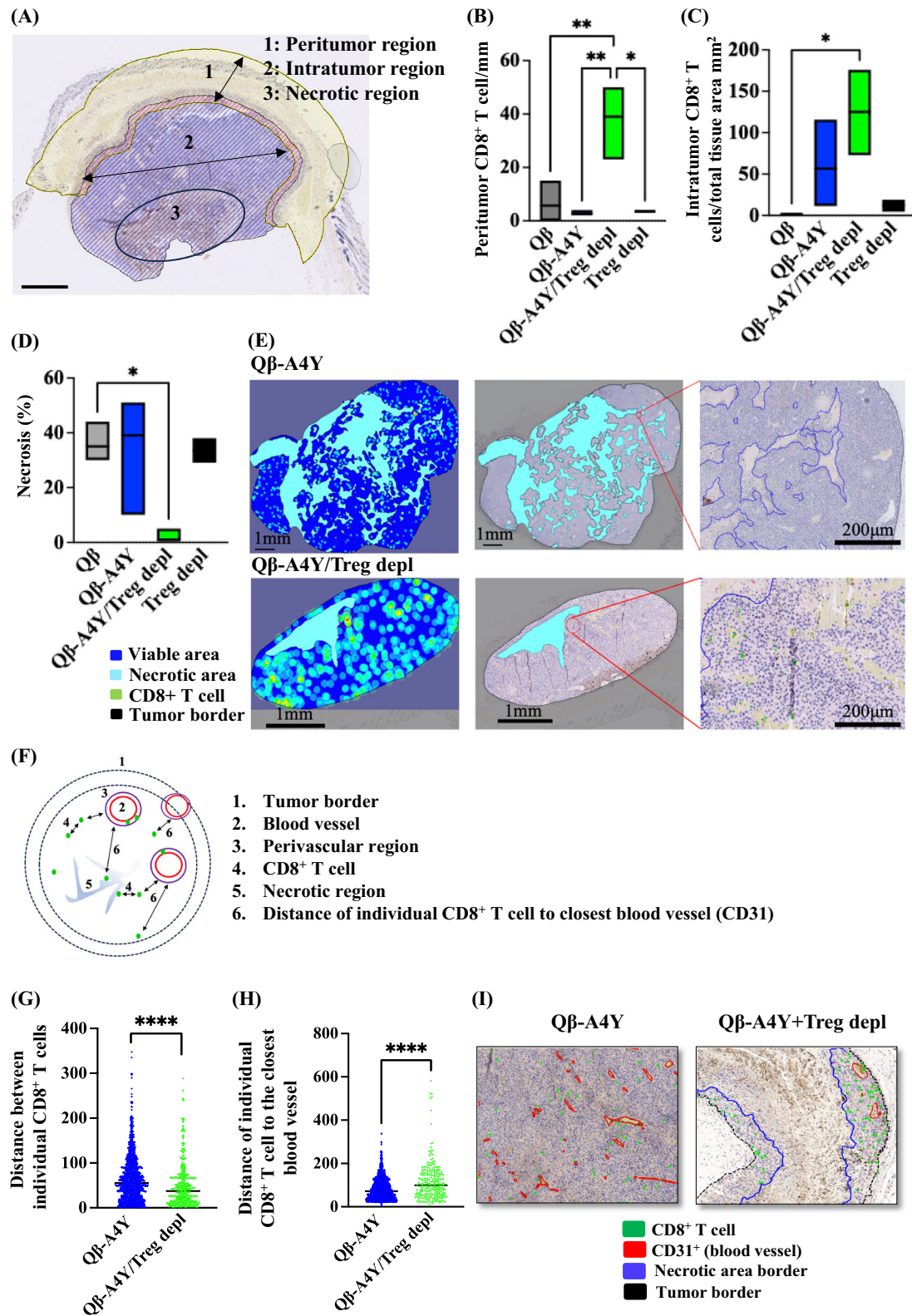
Treg depletion amplifies the effectiveness of vaccines targeting tumor-associated antigens

In a previous study, we utilized immunopeptidomics, bioinformatics, and in vitro T cell stimulation assays, to identify and prioritize TAAs from B16F10 melanoma cells. The TAAs peptides were assessed based on essential physical parameters, including length and affinity to MHC-I ((H2-Db and/or H2-Kb)), with a focus on high-affinity binding peptides¹⁷. Additionally, literature-based evaluation considered key characteristics such as melanocyte specificity or oncogene candidacy. Six peptides including PMEL (VLYRYGSF), MTC-1 (IGIENIHLYL), Calpastatin (SSPANISL), Zinc-finger protein 518B (SSVQNKEYL), Tyrosinase-related protein 2 (SQVMNLHNL) and Caveolin2 (VMYKFLTV) were selected to generate a multitarget vaccine (MTV)¹⁷. To explore the potential of Treg depletion to enhance the antitumor efficacy of natural, usually low-affinity TAAs, we coupled the selected six MHC-I derived-epitopes to Q β (CpGs) using Cu-free click chemistry (Fig. 7A). The efficiency of the coupling was assessed using SDS-PAGE (Fig. 7B). Wild-type C57BL/6 mice were immunized subcutaneously with 120 μ g of MTV, (20 μ g of each vaccine) with or without Treg depletion using 10 μ g of anti-CD25mAb injected intravenously. The priming was performed on day 3, followed by 2 boosts on days 7 and 10 post tumor transplantation (Fig. 7C). Four experimental groups were established: Q β (vehicle control), a group vaccinated with MTV alone, a group receiving MTV vaccination combined with Treg depletion, and a Treg depletion only control group (Fig. 7C). Our results showed that immunization with MTV alone could not hinder tumor progression. However, combining MTV with anti-CD25 mAbs for effective Treg depletion resulted in a significant reduction in tumor volume in comparison to the control groups (Fig. 7D, E). Furthermore, this combination therapy demonstrated enhanced infiltration of CD8⁺ T cells in the tumor (Fig. 7F, G) which also shows enhanced CD8⁺ T cells functionality by IFN- γ production upon stimulation with the six different peptides (Fig. 7H). These data confirm our finding that Treg depletion removes the brake on low-affinity TAAs and enhances their antitumor response.

Discussion

Peptide p33 strongly activates LCMV glycoprotein-specific T cells, including P14 TCR-transgenic T cells²³. In contrast, peptide A4Y has weaker agonistic properties and a reduced ability to activate p33-specific T cells. In this study, we used these two model antigens to investigate the ability of Tregs to specifically suppress antitumor responses of low-affinity agonists such as germline encoded TAAs. To this end, we assessed antitumor responses, cross-reactivity, and protective efficacy against B16F10p33 murine melanoma with or without Treg depletion. To induce strong CTL responses, we generated vaccines based on Q β -VLPs loaded with a strong TLR9 ligand for effective activation of dendritic cells (DCs). Previous studies have shown limited cross-reactivity between p33 and A4Y in P14 TCR-transgenic T cells as well as in a polyclonal setting^{16,24}. We could confirm and extend these findings in vivo by assessing acute lytic activity and antitumor protection demonstrating the limited ability of A4Y-induced T cells to kill p33⁺ target or tumor cells.

Generally, low-affinity T cells can detect and engage with a relatively broad range of antigenic variations, including TAAs. Furthermore, low-affinity T cells are less susceptible to central and peripheral tolerization as compared to high-affinity T cells²⁵. Interestingly, it has recently been shown



that low-affinity CD19 CAR T cells undergo enhanced and prolonged expansion in pediatric patients with acute lymphocytic leukemia²⁶, compatible with the notion that high-affinity T cells are more susceptible to silencing by various mechanisms such as activation-induced cell death²⁷. Thus, induction of T cells with moderate affinity for TAAs may be beneficial. On the other hand, their protective capabilities may be suboptimal. We demonstrate here that low-affinity T cells were indeed inefficient. However,

in the absence of regulatory T cells, the polyclonal population becomes as protective as high-affinity T cells. P33-specific T cells induced by A4Y are expected to have low affinity for A4Y. Hence, our data indicate that the absence of Tregs promotes low-affinity T cells recognizing p33. Conversely, the presence of Tregs selectively suppresses the expansion of these low-affinity T cells. Thus, the absence of Tregs lowers the affinity threshold for T cell activation. Furthermore, we found a significant increase of T_{RM} cells

Fig. 5 | Enhanced tumor infiltration by low-affinity T cells in the absence of Tregs. **A** A tumor image illustrating the measured distances utilizing DL-based histology. 1: peritumor region, 2: Intratumor region and 3: necrotic regions. **B** Number of peritumor CD8⁺ T cells/mm. **C** Number of intratumoral CD8⁺ T cells/total tissue area mm². **D** Percentage of necrosis. **E** Left panel, representative tumors from groups: Q β -A4Y and Q β -A4Y/Treg depl, depicting visual colorization (heat-maps) of CD8⁺ T cells. Regions with high positive CD8 cell counts ('hot') are circled in red, while areas with the lowest positive cell counts are displayed in light blue ('cold'). The tumor border is delineated by a dashed black line, areas of tumor necrosis are marked in light blue, and dark blue is viable tumor areas. The middle and right panels show IHC staining of the same representative tumors, highlighting a hotspot area (circled

in red) of CD8⁺ T cells (green). **F** A cartoon illustrating the measured distances utilizing DL-based histology. 1 = Tumor border, 2 = Blood vessel, 3 = Perivascular region, 4 = Distance of individual CD8⁺ T cell to another CD8⁺ T cell, 5 = Necrotic region border, 6 = Distance of individual CD8⁺ T cell to closest blood vessel (CD31). **G** Distance measurement between individual CD8⁺ T cells in the tumor, each dot represents a different distance. **H** Distance of individual CD8⁺ T cell to the closest blood vessel. Each dot represents a different distance. **I** Representative IHC staining of tumor in mice vaccinated with Q β -A4Y or Q β -A4Y/Treg depl, depicting CD8⁺ T cells in green, CD31⁺ (blood vessel) in red, necrotic regions in blue and tumor border in black. Statistical analysis with Student's *t*-test. The sample size for each group was *n* = 3.

after vaccination with the low-affinity vaccine and Treg depletion, highlighting the role of Tregs in hindering the efficacy of low-affinity T cells. T_{RM} cells, characterized by the expression of CD103 [α_E (CD103) β_7] integrin, are strategically positioned in peripheral tissues, and continuously monitor pathogen invasions and tumor progression²⁸. T_{RM} cells are enabling a rapid and potent local defense against recurrence and contributing to long-term immune resilience. The molecule CD103 plays a crucial role as it binds to E-cadherin. This interaction promotes the retention of T_{RM} within epithelial tumor islets and enhances the maturation of cytotoxic immune synapses with cancer cells²⁹. Our data regarding the role of T_{RM} cells suggests their potential involvement in protective immunity, but further research is needed to confirm their exact protective behavior in the context of our study. In our previous work, we demonstrated that Q β -VLPs packaged with CpG oligonucleotides (TLR9 ligands) effectively activate DCs and their subsets within tumors. Building on these findings, we now plan to explore in greater detail the combined effects of low-affinity VLP-based vaccines, packaged with CpGs, and Treg depletion on the expansion of DCs³⁰.

The significance of the spatial distribution of CD8⁺ T cells within tumors, quantified by the "Immunoscore," is crucial for cancer prognosis³¹. This concept emphasizes that a better outcome is associated with the presence of CD8⁺ T cells both at the core and at the invasive edges of the tumor. This dual presence at both locations is more favorable compared to their localization in just one of these areas³². Through the application of DL-based histology learning techniques, we show here that removing the brake on low-affinity T cells by removing Tregs leads to increased T cell infiltration in the peritumoral area and to a lesser extent intratumorally. A larger sample number may be needed to demonstrate a difference against the other treatment groups. Q β -A4Y vaccine with Treg depletion was also effective in reducing tumor necrosis. Interestingly, a recent study examining colorectal cancer highlighted the immunological and prognostic importance of tumor necrosis. It revealed that a higher percentage of tumor necrosis is associated with reduced cancer-specific survival, independent of tumor grade, mutations, or other confounding factors³³. The evidence of increased tumor cell death indicates a more aggressive cancer, which can be explained by rapid tumor growth that has outgrown its blood supply³⁴. Interestingly, Treg depletion not only brought CD8⁺ T cells into closer contact within the tumor but also facilitated their deeper penetration from blood vessels into the tumors as shown by AI-assisted quantitative histology. Together, the combination of the low-affinity vaccine with Treg depletion led to improved infiltration of the tumor by CD8⁺ T cells, resulting in improved antitumor protection.

Ahmed et al. demonstrated that depleting Treg cells in LCMV infection led to an expansion of functional LCMV-specific CD8 T cells but did not reduce viral load³⁵. Additionally, Treg cell depletion resulted in a significant increase in PD-L1 expression on infected cells, and combining Treg depletion with PD-L1 blockade significantly reduced viral titers. Based on these findings, we plan to investigate this approach in our future research, exploring the potential of combining Treg depletion with anti-PD-L1 blockade to enhance the activation of low-affinity T cells in cancer vaccines.

In general, cross-reactivity is often observed among nearly identical peptides, differing by only 1 or 2 amino acids, particularly evident in MHC-I epitopes of 8-10 amino acids³⁶. We observed an enhanced cross-reactive

response in the blood following Treg depletion in mice bearing B16F10p33, especially in conjunction with the low-affinity Q β -A4Y vaccine. The enhanced cross-reactive response was even more pronounced within the tumors. Overall, p33-cross-reactive T cells were enriched in the tumor compared to the blood after A4Y-immunization; this increase was further accentuated in the absence of Tregs, indicating that the presence of p33 in the tumor enriched for p33-cross-reactive T cells. In general, translating Treg depletion strategies in combination with low-affinity cancer vaccine to humans may carry some risks, including the possibility of immune-related toxicity, particularly in the context of broader T cell cross-reactivity, as observed in our study. Therefore, careful optimization of dosing, timing, and targeting will be essential to minimize undesired inflammation in future clinical applications. On the other hand, extended experience from various immunotherapies including CTLA-4 blockade suggests that such inflammatory side-effects can clinically be managed.

Petreman et al. have recently profiled a large library of CD8⁺ T cells specific for TAAs, including neoantigens and viral epitopes, from tumors and blood samples of healthy donors and patients with solid tumors. Although neoantigen-specific T cells typically exhibited higher avidity than those specific to other TAAs, a broad range of avidities were still observed³⁷. Some neoantigen-specific clonotypes exhibited suboptimal, low-avidity TCRs³⁸. Therefore, some TCRs specific for neoantigens are also of low-to-moderate avidity, suggesting that it may generally be useful to promote tumor infiltration of such T cells. Whether this applies also to checkpoint inhibition and adoptive transfer therapy with TILs remains to be shown. Our findings demonstrates that TAAs-based vaccines effectively impedes the progression of B16F10 melanoma when combined with Treg depletion. This approach increased CD8⁺ T cell infiltration in the tumor and enhanced their ability to protect against tumor growth.

Methods

Generation of VLP vaccines

Bacteriophage VLP-Q β were used as a vaccine platform. The cultivation and purification of Q β -VLPs were conducted as previously described^{17,18,30,39}. The naturally packaged ssRNA within Q β during the expression process⁴⁰ was enzymatically digested and subsequently repackaged with type-B CpGs (5'-TCC ATG ACG TTC CTG ATG CT-3') (Invitrogen) as outlined in reference¹⁸. The successful packaging was confirmed using a 1% agarose gel stained with SYBR Safe and Coomassie Blue. Following the packaging step, Q β (1668)-VLPs (hereafter Q β) were derivatized using dibenzocyclooctyne NHS ester (DBCO cross-linker, Sigma-Aldrich) for 30 min at room temperature, using 4-fold molar excess. Excess DBCO cross-linker was removed using Amicon-Ultra 0.5 ml tubes with 100 kDa molecular weight cut-off (MWCO). p33 (H-KAVYNFATMKN3-NH2) and A4Y (H-KAVANFATMKN3-NH2) peptides were synthesized by (Biosynth AG) with the addition of a lysine and an azide group at the C-terminus to facilitate efficient coupling to derivatized Q β . The peptides were reconstituted in Dimethyl Sulfoxide (DMSO) and added in a 2-fold excess over Q β (each vaccine was generated separately). The resulting mixture was incubated for 1 h at room temperature on a shaker at 450 round-per-minute (rpm), and the excess uncoupled peptide was removed using an Amicon-Ultra 0.5 ml tube with a 100 kDa MWCO. The efficiency of the coupling was assessed

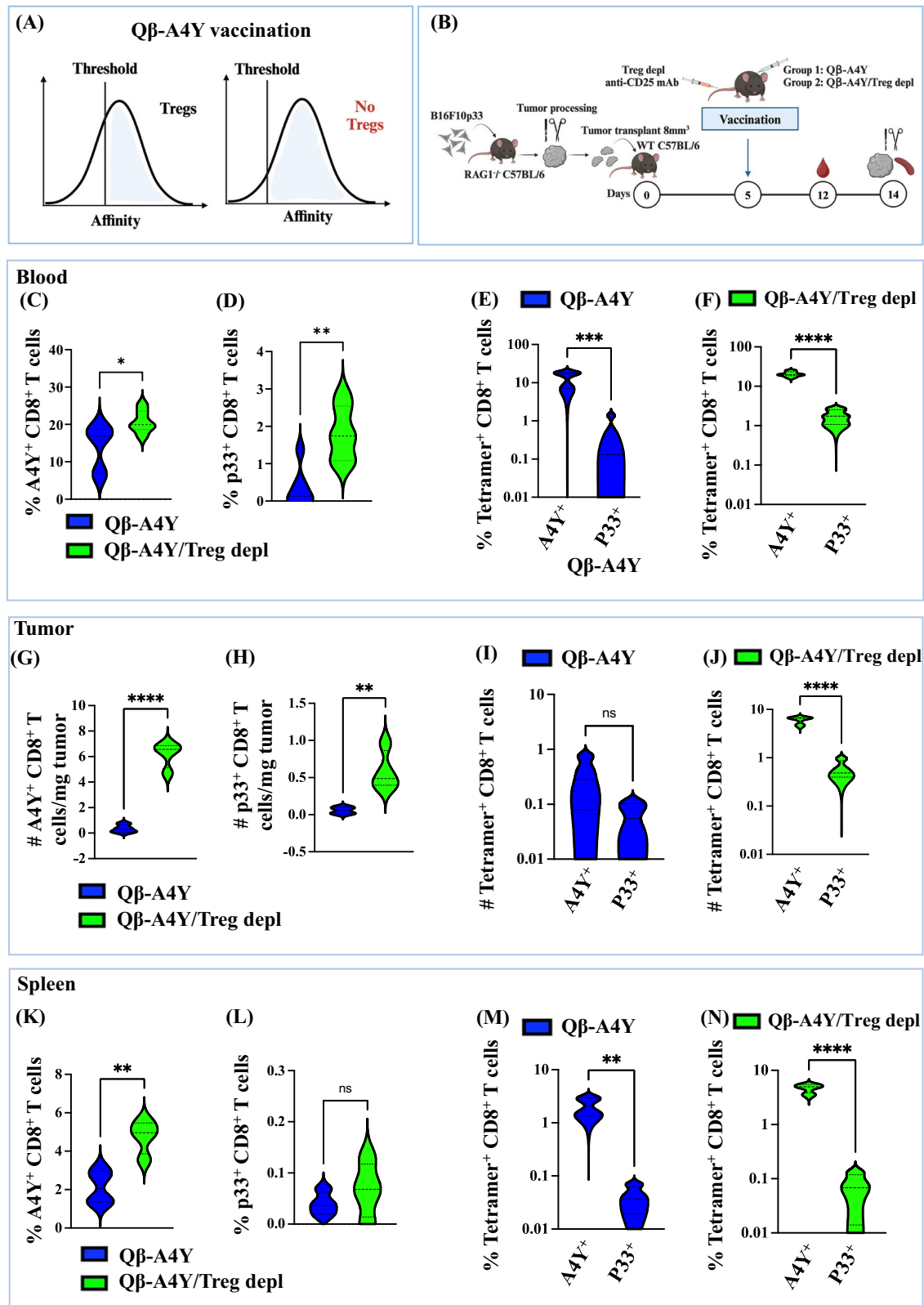
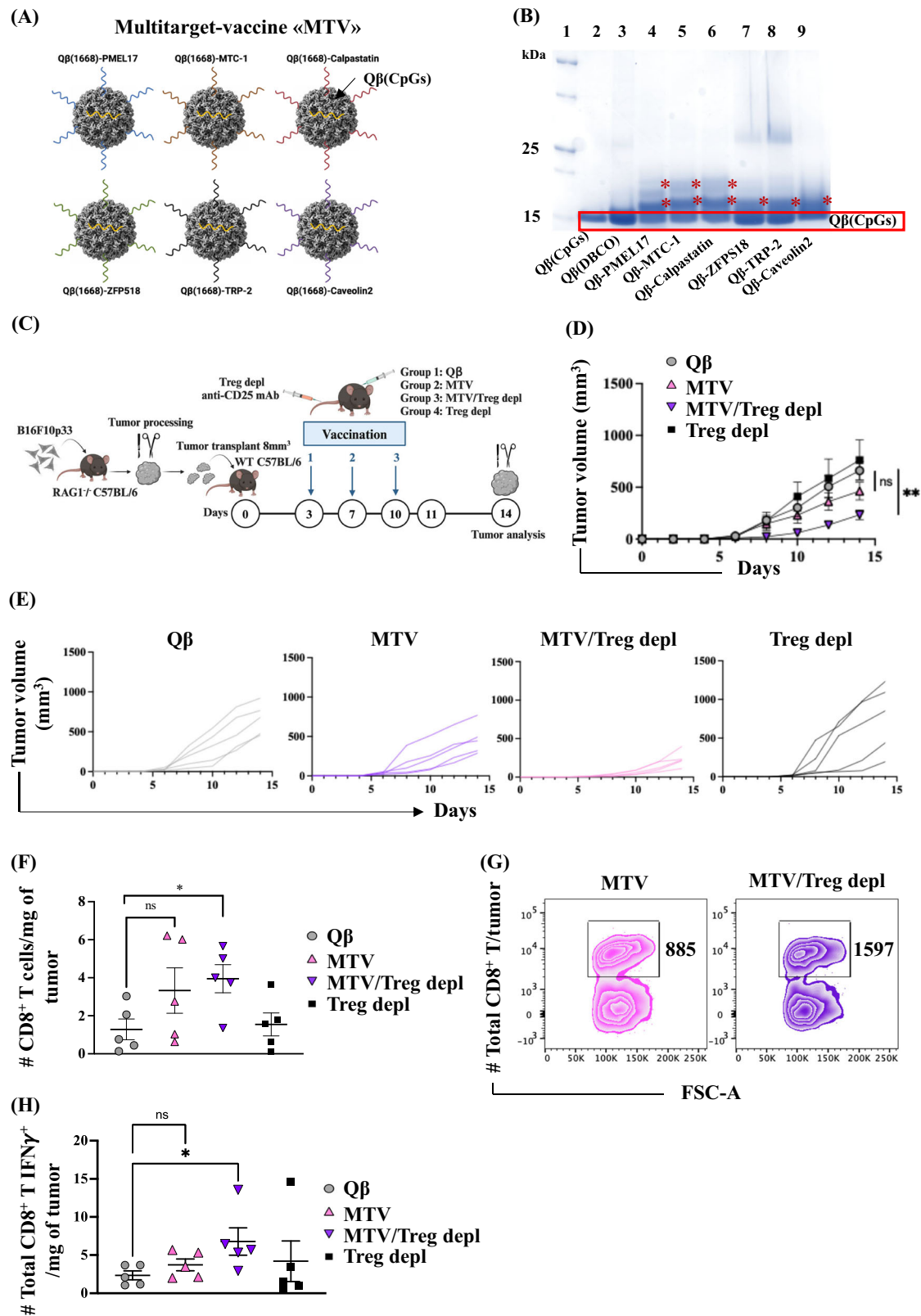


Fig. 6 | Depletion of Tregs enhances cross-reactivity. A A diagram illustrating the activation of cross-reactive T cells following vaccination with low-affinity Qβ-A4Y, either alone or in combination with Treg depletion. B An illustration depicting the vaccination regimen using one vaccination dose administered 5 days following tumor transplantation. Two groups were established: Qβ-A4Y and Qβ-A4Y/Treg depl. C, D Percentage of A4Y⁺ and p33⁺ T cells within CD8⁺ T cells in the blood, measured 7 days post-vaccination with Qβ-A4Y or Qβ-A4Y/Treg depl. E, F An

alternative way of presenting data in (C, D). G, H Densities of A4Y⁺ and p33⁺ T cells within CD8⁺ T cells in the tumors measured on day 14. I, J An alternative way of presenting data in (G, H). K, L Percentage of A4Y⁺ and p33⁺ T cells within CD8⁺ T cells in the spleen, measured on day 14. M, N An alternative way of presenting data in (K, L). Statistical analysis with Student's *t*-test. The sample size for each group was *n* = 6.



using SDS-PAGE (BioRad) and 1% agarose gel. The generation of the germline (TAAs) multitarget vaccine (MTV) was carried out following the detailed procedure outlined in ref. 17 using Qβ(1668)-VLPs as a platform. The MTV vaccine consists of 20 µg of each of the following peptides: melanocyte protein PMEL (VLYRYGSF), MTC-1 (IGIENIHYL),

Calpastatin (SSPANISL), Zinc-finger protein 518B (SSVQNKEYL), Tyrosinase-related protein 2 (SQVMNLHNL) and Caveolin2 (VMYKFLTV). The selected TAAs epitopes of B16F10 melanoma cells were identified using immunopeptidomics and whole exome sequencing. The length distribution of selected peptides were 8 and 9 amino acids¹⁷.

Fig. 7 | Treg depletion amplifies the effectiveness of vaccines targeting tumor-associated antigens. **A** A cartoon illustrating the generated multitarget vaccine (MTV) consisting of six CD8⁺ T-cell germline epitopes of B16F10 melanoma cells that were identified using immunopeptidomics and whole exome sequencing. The length distribution of the selected peptides was 8 and 9 amino acids¹⁷. **B** SDS-PAGE stained with Coomassie Blue, with Lane 1, protein marker; Lane 2, Q β (CpGs) at 14 kDa; and Lane 3, Q β (CpGs) derivatized with a dibenzocyclooctyne bifunctional cross-linker (DBCO), Lanes 4–9 show coupling to TAAs peptides: PMEL (VLYRYGSF), MTC-1 (IGIENIHYL), Calpastatin (SSPANISL), Zinc-finger protein 518B (SSVQNKEYL), Tyrosinase-related protein 2 (SQVMNLHNL) and Caveolin2 (VMYKFLTV) respectively. Red box indicates Q β (CpGs) monomer before and after derivatization with DBCO and coupling to peptides. Black arrows indicate the

coupled peptides to the Q β monomer. **C** An illustration depicting the vaccination regimen with MTV administered following transplantation of B16F10p33 tumors, combined with intravenous injection of anti-CD25 mAb for effective depletion of Tregs. Four experimental groups were established: Q β (control), a group vaccinated with MTV alone, a group receiving MTV vaccination combined with Treg depletion (MTV/Treg depl), and a Treg depletion control group. **D** Tumor volume mm³. **E** Tumor volume mm³ of individual mice. **F** Density of CD8⁺ T cells in the tumors. **G** Representative flow cytometry plots illustrating the total number of CD8⁺ T cells acquired from a tumor in each group. **H** Density of IFN- γ producing CD8⁺ T cells in the tumor. Stimulation was conducted using a mixture of peptides. Statistical analysis with Student's *t*-test. The sample size for each group was *n* = 5.

Mice

In all experiments, we utilized wild-type C57BL/6 female mice aged 8–12 weeks, which were purchased from Harlan and kept in the central animal facility (CAF) at the Department of BioMedical Research of the University of Bern. RAG1^{-/-} C57BL/6 mice were bred in the CAF. All animal experiments were conducted in strict adherence to the Swiss Animal Act (455.109.1, September 2008, 5th edition) and were carried out under the approved licenses BE10/18, BE43/21 and BE30/24.

Vaccination doses and regimens

The vaccine was administered in all experiments subcutaneously in the loose back skin of the neck area. The administered vaccination dose remained constant across all experiments, with each dose consisting of 50 μ g of either Q β (control), Q β -p33, or Q β -A4Y, all diluted in a final volume of 100 μ l PBS. The vaccination dose for the MTV is 120 μ g per dose comprising 20 μ g of each vaccine: melanocyte protein PMEL (VLYRYGSF), MTC-1 (IGIENIHYL), Calpastatin (SSPANISL), Zinc-finger protein 518B (SSVQNKEYL), Tyrosinase-related protein 2 (SQVMNLHNL) and Caveolin2 (VMYKFLTV), diluted in a final volume of 100 μ l PBS/dose.

Measuring tetramer⁺ T cell response

P33 (KAVYNFATM) and A4Y (KAVANFATM) specific tetramers were designed with H-2D^b allele and labeled with PE or APC fluorochromes (MBL company). Blood and spleen were collected and processed using a 70 μ m cell strainer (Sigma-Aldrich). The isolated cells were washed once with sterile PBS, and RBCs were lysed using 500 μ l of Ammonium-Chloride-Potassium (ACK) buffer (0.155 M Ammonium chloride, 0.01 M Kaliumhydrogencarbonat, 0.1 M EDTA) on ice for 2–3 min. Approximately, one million cells were collected in a 96-well V-bottom plate and stained with anti-mouse CD16/32 mAbs (clone 2.4G2, BD Bioscience) for 10 min in the dark. Plates were then centrifuged, and cells were stained with live/dead 7-AAD, p33 tetramer, or A4Y tetramer for 20 min in the dark, followed by anti-mouse CD8 α mAb (clone 53–6.7, BD Biosciences). For T_{RM} cells staining, tissues were collected and processed like tumor samples. Anti-mouse CD62L mAb (clone MEL-14, BD Bioscience) and anti-mouse CD103 mAb (M290, BD Bioscience) were used. After spinning, plates were centrifuged, and a single-cell suspension was prepared for flow cytometry analysis using BD[®] LSR II Flow Cytometer. Data were analyzed using FlowJo X version 10.9.0. All monoclonal antibodies were diluted to a concentration of 1:300 while tetramers were diluted at 1:50. The gating strategy for blood or spleen samples involved a sequential selection of singlets, live/dead cells, lymphocytes, CD8⁺ T cells and further categorized into A4Y⁺ or p33⁺ T cells using tetramer staining (Suppl. Fig. 1A).

Intracellular-cytokine staining

Intracellular cytokine staining was performed using spleens or TILs collected from mice to measure the levels of IFN- γ secretion (absolute numbers or density). TILs collection is described in the method section. Approximately 1 million cells were isolated from the spleen while for TILs, all cells were collected to measure the density. The densities were determined by calculating the ratio of the total number of the specific-cell population

within each tumor to the tumor weight in mg. Collected splenocytes or TILs were pulsed with 1 ng of A4Y for 6 h at 37 °C in the presence of Brefeldin A and Monensin (BD Biosciences) at a 1:1000 dilution. Following the incubation, the cells were collected and washed 3 times with sterile PBS containing 0.1% BSA and seeded in a 96-well V-bottom plate. The Fc receptor blocking was carried out using anti-mouse CD16/32 mAbs (clone 2.4G2, BD Bioscience) for 10 min in the dark, then centrifuged at 1200 rpm for 5 minutes and the supernatant was discarded. Cells were next stained with live/dead 7-AAD, A4Y tetramer (MBL company), anti-mouse CD8 α mAb (clone 53–6.7, BD Biosciences) for 20 min in the dark, centrifuged at 1200 rpm for 5 min; the supernatant was discarded. The cells were fixed using 100 μ l of the fixation buffer (BD Cytofix) at 4 °C for 15 min. The plate was centrifuged at 1200 rpm for 5 min; the supernatant was discarded; and TILs were washed with 100 μ l of 1 \times diluted permeabilization wash buffer (BioLegend) and centrifuged immediately at 1200 rpm for 5 min; the supernatant was discarded. TILs were then stained with anti-mouse IFN- γ mAb (clone XMGI.2, MERCK). Plates were centrifuged at 1200 rpm for 5 min; the supernatant was discarded; TILs were resuspended in PBS and 0.1% BSA and added to 5 mL round-bottom tubes with a cell strainer to remove excess tumor debris. Samples were read by FACSCaliber or LSR-II and analysis was done using GraphPad Prism V.8.4.2 (464). A similar procedure was used for assessing IFN- γ production after vaccination with the MTV without tetramer staining. Stimulation was performed using 1 μ g of a mixture of the six different peptides. No stimulation controls were added. All monoclonal antibodies were diluted to a concentration of 1:300 while tetramers were diluted at 1:50.

CFSE cytolytic assay

Wild-type C57BL/6 mice were vaccinated subcutaneously with 50 μ g of Q β -A4Y or Q β -p33 vaccines. Control mice received only Q β . Eight days after vaccination, splenocytes from naïve wild-type C57BL/6 mice were collected and RBCs were lysed. Naïve splenocytes were pulsed with 1 ng of p33 or A4Y peptides, along with 10 μ M carboxyfluorescein succinimidyl ester (CFSE). Previously vaccinated mice were injected intravenously with 1 million pulsed/labeled cells. Four hours later, the spleens of the vaccinated mice were collected, processed, and analyzed using flow cytometry to determine the percentage of CFSE-labelled cells for each experimental group. The percentage of lytic activity was measured using the formula: 1- (% of CFSE-pulsed splenocytes in vaccinated mice/% CFSE-pulsed splenocytes in control mice) \times 100. Please note that negative lytic activity normally occurs in this type of analysis.

Tumor experiments

One million B16F10p33 melanoma cells were injected into the flank of RAG1^{-/-} C57BL/6 mice. Tumors were allowed to grow for 14 days until they reached 1 cm³. Tumors were resected and processed into ~8 mm³ fragments and kept in complete medium (DMEM + 10% FBS + 1% Pen-Strep) on ice. A tumor fragment was then implanted into a flank of wild-type C57BL/6 mice (8–12 weeks old, Harlan) under full anesthesia. The anesthesia of animals was carried out according to the animal License BE43/21 and BE30/24 with a narcotic mixture (Domitor 0.4 mg/kg, Dormicum 4 mg/kg, Fentanyl 0.04 mg/kg). The implanted tumor was allowed to grow

for 3 days before treatment started. Vaccines were given subcutaneously 3 times over 14 days as indicated in the results section. Tumor growth was monitored every 2 days and measured using calipers. Mice were monitored every day to assess tumor growth and overall health status. Tumors were measured using calipers with the formula $V = (W \times W \times L)/2$, V = final tumor volume in mm³, L = tumor length, and W = tumor width. On day 14, mice were euthanized as tumors in the control group reached the humane endpoint. Euthanasia of animals was carried out using CO₂ and decapitation. Tumors were harvested and the weight was recorded in mg. The collected tumors were digested by DNaseI (Boehringer) and collagenase D (Roche) in DMEM for 1 h at 37 °C. Next, tumors were cut into smaller pieces, and then processed through a 70 µm cell strainer. Throughout this process, cells were consistently washed using complete DMEM in Falcon 50 ml tubes. The collected cells were added to 15 ml tubes containing 2 ml of 35% Percoll and then centrifuged at 1800 rpm for 25 min at room temperature to isolate TILs. Subsequently, TILs were resuspended in 200 µl of PBS with 0.1% BSA (flow cytometry buffer), and the suspension was transferred to 96-well V-bottom plate. Staining of TILs was performed as described earlier. Plates were centrifuged at 1200 rpm for 5 min, the supernatant was removed, and TILs were resuspended in flow cytometry buffer. Subsequently, they were transferred to 50 ml round-bottom tubes through a cell strainer to eliminate any excess tumor debris. The samples were analyzed using a BD[®] LSR II Flow Cytometer and data analysis was conducted with GraphPad Prism (version 8.4.2). The tumor densities were determined by calculating the ratio of the total number of the specific cell population within each tumor to the corresponding tumor weight in mg. All mAbs were diluted to a concentration of 1:300 while tetramers were diluted at 1:50. The gating strategy involved a sequential selection of singlets, live/dead cells, lymphocytes, CD8⁺ T cells and further categorized into A4Y⁺ or p33⁺ T cells using tetramer staining (Suppl. Fig. 1B).

Treg depletion

To deplete Tregs, 10 µg of anti-mouse CD25 (clone PC61, Biolegend) was injected intravenously. Throughout the text, the terms “anti-CD25” mAb or “Treg depletion/Treg depl” are used interchangeably. Treg depletion was assessed in the blood 48 h following intravenous injection. Blood samples were processed as described earlier. Staining of Tregs was carried out using anti-mouse CD4 mAb (clone RM4-5, eBioscience), anti-mouse CD25 mAb (clone CD25-4E3, BD Bioscience) and anti-mouse FOXP3 (clone MF23, BD Bioscience). All monoclonal antibodies were diluted to a concentration of 1:300. The gating strategy used involved a sequential selection of singlets, live/dead cells, lymphocytes, CD4⁺ T cells, CD25⁺ followed by FOXP3⁺ cells (Fig. 3B).

High dimensional analysis of flow cytometry data

High dimensional analysis of flow cytometry data has been performed using t-distributed stochastic neighbor embedding (tSNE) and FlowSOM clustering and isualization technique for T_{RM} cells for the group vaccinated with Qβ-A4Y/Treg depl. The gating strategy involved a sequential selection of singlets, live cells, lymphocytes, and CD8⁺ T cells using FlowJo X version 10.4.2. Five different compensated FCS files were exported (5 different samples in each group) and then concatenated. FCS files included a consistent number of events. For FlowSOM analysis, five clusters were selected to assess specific marker expression (CD8, A4Y tetramer, CD69, CD62L, and CD103).

Histology

For microscopic analysis, tumor samples were collected on day 14 post tumor transplantation. The samples were measured and weight was recorded in mg and then fixed in buffered 4% formalin for 24 h and routinely processed and stained with HE for histologic examination. IHC was performed for anti-mouse CD8 (clone 4SM15, eBioscience) and anti-mouse CD31 (AF3628-SP, R&D Systems), as single and double staining. Histology slides were scanned for digital analysis by a board-certified veterinary pathologist (SdB) (NanoZoomer S360MD Slide scanner system; Hamamatsu Photonics, Shizuoka, Japan). Detection and quantification of tumor tissue, tumor necrosis, CD8⁺

cells, and CD31⁺ vessels were performed digitally using a DL-based histology software (Visiopharm, Hørsholm, Denmark). The absolute and relative (% of the entire tumor tissue section) area of tumor necrosis were calculated. For the quantification of tumor vascularization, the (individual and total) tissue area comprising blood vessels and the vessel count (vascular density) was measured. The total number of CD8⁺ cells was determined, and relative counts were calculated per mm (tumor periphery) and mm² (intratumoral region). For each CD8⁺ cell, the closest distance to another CD8⁺ cell, a blood vessel, and the tumor border was measured. Based on the CD8⁺ cell counts, heat maps (visual colorization) were generated for the visualization of the spatial distribution of these T cells.

Statistics

Data are expressed as mean ± SEM. Statistical analysis was performed using one-way ANOVA and Student's *t*-test (two-tailed). In result 7, Student's *t*-test (two-tailed) where each experimental group was compared to the control group vaccinated with Qβ was used as a baseline. Tumor-free survival was analyzed utilizing the Log-rank (Mantel-Cox) test, the median survival in days and the survival rate at days 49 and 100. Significance levels are denoted as follows: *****p* < 0.0001; ****p* < 0.001; ***p* < 0.01; **p* < 0.05. Refer to the figure legends for detailed information regarding the performed analyses.

Data availability

All data supporting the findings of this study are contained within the article and its supplementary content. The raw data can be obtained from the corresponding author upon reasonable request.

Received: 2 August 2024; Accepted: 20 May 2025;

Published online: 13 June 2025

References

1. Lanzavecchia, A. & Sallusto, F. Antigen decoding by T lymphocytes: from synapses to fate determination. *Nat. Immunol.* **2**, 487–492 (2001).
2. Bachmann, M. F. & Kopf, M. Balancing protective immunity and immunopathology. *Curr. Opin. Immunol.* **14**, 413–419 (2002).
3. Lyons, D. S. et al. A TCR binds to antagonist ligands with lower affinities and faster dissociation rates than to agonists. *Immunity* **5**, 53–61 (1996).
4. Sabatino, J. J. Jr., Huang, J., Zhu, C. & Evavold, B. D. High prevalence of low affinity peptide-MHC II tetramer-negative effectors during polyclonal CD4⁺ T cell responses. *J. Exp. Med.* **208**, 81–90 (2011).
5. Martinez, R. J. & Evavold, B. D. Lower affinity T cells are critical components and active participants of the immune response. *Front. Immunol.* **6**, 468 (2015).
6. Coulie, P. G., Van den Eynde, B. J., van der Bruggen, P. & Boon, T. Tumour antigens recognized by T lymphocytes: at the core of cancer immunotherapy. *Nat. Rev. Cancer* **14**, 135–146 (2014).
7. Brossart, P. & Bevan, M. J. Selective activation of Fas/Fas ligand-mediated cytotoxicity by a self peptide. *J. Exp. Med.* **183**, 2449–2458 (1996).
8. Brossart, P. Antitumor immunity and T-cell avidity. *Blood* **136**, 378–380 (2020).
9. Selck, C. & Dominguez-Villar, M. Antigen-specific regulatory T cell therapy in autoimmune diseases and transplantation. *Front. Immunol.* **12**, 661875 (2021).
10. Gregori, S., Goudy, K. S. & Roncarolo, M. G. The cellular and molecular mechanisms of immuno-suppression by human type 1 regulatory T cells. *Front. Immunol.* **3**, 30 (2012).
11. Lathrop, S. K. et al. Peripheral education of the immune system by colonic commensal microbiota. *Nature* **478**, 250–254 (2011).
12. Whitehead, G. S. et al. IL-35 production by inducible costimulator (ICOS)-positive regulatory T cells reverses established IL-17-dependent allergic airways disease. *J. Allergy Clin. Immunol.* **129**, 207–15 e1–5 (2012).
13. Ye, S. et al. Peripheral lymphocyte populations in ovarian cancer patients and correlations with clinicopathological features. *J. Ovarian Res.* **15**, 43 (2022).

14. Fang, R. et al. Significance of peripheral blood Tregs in tumor: a narrative review. *Ann. Blood*. **5**, 34–44 (2020).
15. Zhulai, G. & Oleinik, E. Targeting regulatory T cells in anti-PD-1/PD-L1 cancer immunotherapy. *Scand. J. Immunol.* **95**, e13129 (2022).
16. Bachmann, M. F. et al. T cell responses are governed by avidity and co-stimulatory thresholds. *Eur. J. Immunol.* **26**, 2017–2022 (1996).
17. Mohsen, M. O. et al. Targeting mutated plus germline epitopes confers pre-clinical efficacy of an instantly formulated cancer nano-vaccine. *Front. Immunol.* **10**, 1015 (2019).
18. Mohsen et al. Bedside formulation of a personalized multi-neoantigen vaccine against mammary carcinoma. *J. Immunother. Cancer* **10**, e002927 (2022).
19. Mohsen, M. O. et al. Vaccination with nanoparticles combined with micro-adjuvants protects against cancer. *J. Immunother. Cancer* **7**, 114 (2019).
20. Mohsen, M. O. et al. In situ delivery of nanoparticles formulated with micron-sized crystals protects from murine melanoma. *J. Immunother. Cancer* **10**, e004643 (2022).
21. Wu, Y. et al. A local human V δ 1 T cell population is associated with survival in nonsmall-cell lung cancer. *Nat. Cancer* **3**, 696 (2022). +.
22. Hiraoka, N. et al. Tumour necrosis is a postoperative prognostic marker for pancreatic cancer patients with a high interobserver reproducibility in histological evaluation. *Br. J. Cancer* **103**, 1057–1065 (2010).
23. Boulter, J. M. et al. Potent T cell agonism mediated by a very rapid TCR/pMHC interaction. *Eur. J. Immunol.* **37**, 798–806 (2007).
24. Böttig, P., Saudan, P., Storni, T., Gallimore, A. & Bachmann, M. F. Limited in vivo reactivity of polyclonal effector cytotoxic T cells towards altered peptide ligands. *Microbes Infect.* **7**, 729–737 (2005).
25. Waldman, A. D., Fritz, J. M. & Lenardo, M. J. A guide to cancer immunotherapy: from T cell basic science to clinical practice. *Nat. Rev. Immunol.* **20**, 651–668 (2020).
26. Ghorashian, S. et al. Enhanced CAR T cell expansion and prolonged persistence in pediatric patients with ALL treated with a low-affinity CD19 CAR. *Nat. Med.* **25**, 1408–1414 (2019).
27. Green, D. R., Droin, N. & Pinkoski, M. Activation-induced cell death in T cells. *Immunol. Rev.* **193**, 70–81 (2003).
28. Hardenberg, J. B., Braun, A. & Schon, M. P. A Yin and Yang in epithelial immunology: the roles of the alpha(E)(CD103)beta(7) integrin in T cells. *J. Invest. Dermatol.* **138**, 23–31 (2018).
29. Corgnac, S., Boutet, M., Kfoury, M., Naltet, C. & Mami-Chouaib, F. The emerging role of CD8(+) tissue resident memory T (T(RM)) cells in antitumor immunity: a unique functional contribution of the CD103 integrin. *Front. Immunol.* **9**, 1904 (2018).
30. Josi et al. A tetravalent nanovaccine that inhibits growth of HPV-associated head and neck carcinoma via dendritic and T cell activation. *iScience* **27**, 109439 (2024).
31. Angell, H. & Galon, J. From the immune contexture to the Immunoscore: the role of prognostic and predictive immune markers in cancer. *Curr. Opin. Immunol.* **25**, 261–267 (2013).
32. Pages, F. et al. In situ cytotoxic and memory T cells predict outcome in patients with early-stage colorectal cancer. *J. Clin. Oncol.* **27**, 5944–5951 (2009).
33. Kastinen, M. et al. Immunological and prognostic significance of tumour necrosis in colorectal cancer. *Br. J. Cancer* **128**, 2218–2226 (2023).
34. Szabó, A. & Merks, R. M. H. Blood vessel tortuosity selects against evolution of aggressive tumor cells in confined tissue environments: a modeling approach. *Plos Comput Biol.* **13**, e1005635 (2017).
35. Penalzoza-MacMaster, P. et al. Interplay between regulatory T cells and PD-1 in modulating T cell exhaustion and viral control during chronic LCMV infection. *J. Exp. Med.* **211**, 1905–1918 (2014).
36. Gouttefangeas, C., Klein, R. & Maia, A. The good and the bad of T cell cross-reactivity: challenges and opportunities for novel therapeutics in autoimmunity and cancer. *Front. Immunol.* **14**, 1212546 (2023).
37. Petremand, R. et al. Identification of clinically relevant T cell receptors for personalized T cell therapy using combinatorial algorithms. *Nat. Biotechnol.* **43**, 323–328 (2024).
38. Petremand R., et al. Author Correction: Identification of clinically relevant T cell receptors for personalized T cell therapy using combinatorial algorithms. *Nat. Biotechnol.* **43**, 445 (2024).
39. Josi, R. et al. Intranodal injection of immune activator demonstrates antitumor efficacy in an adjuvant approach. *Vaccines (Basel)*. **12**, 355 (2024).
40. Chang, X. Y. et al. TLR7 signaling shapes and maintains antibody diversity upon virus-like particle immunization. *Front. Immunol.* **12**, 827256 (2022).

Acknowledgements

This research was funded by Swiss National Foundation (SNF): (Grant Number: 320030-228094), Swiss Cancer Research (Grant Number KFS-5246-02-2021-R) and Jubiläumsstiftung von Swiss Life. Illustrations were generated with BioRender.com.

Author contributions

Design of experiments, acquisition of data, interpretation, and analysis of data: M.O.M., R.J., A.G., S.M., Y.L., A.S.C., S.M., P.K., Sd.B., and M.F.B. Writing, revision and editing of paper: M.O.M., D.E.S., Sd.B., and M.F.B. Technical, material and tool support: M.F.B. and M.O.M. Histology and IHC: Sd.B., M.O.M. Study supervision: M.O.M. and M.F.B. All authors read and approved the final paper.

Competing interests

M.O.M., D.E.S., and M.F.B. have financial interests as shareholders in DeepVax GmbH, a company that specializes in the development of cancer immunotherapy. DeepVax GmbH is a spinoff from the University of Bern. The remaining authors declare no competing interests.

Additional information

Supplementary information The online version contains supplementary material available at <https://doi.org/10.1038/s41541-025-01177-y>.

Correspondence and requests for materials should be addressed to Mona O. Mohsen.

Reprints and permissions information is available at <http://www.nature.com/reprints>

Publisher's note Springer Nature remains neutral with regard to jurisdictional claims in published maps and institutional affiliations.

Open Access This article is licensed under a Creative Commons Attribution-NonCommercial-NoDerivatives 4.0 International License, which permits any non-commercial use, sharing, distribution and reproduction in any medium or format, as long as you give appropriate credit to the original author(s) and the source, provide a link to the Creative Commons licence, and indicate if you modified the licensed material. You do not have permission under this licence to share adapted material derived from this article or parts of it. The images or other third party material in this article are included in the article's Creative Commons licence, unless indicated otherwise in a credit line to the material. If material is not included in the article's Creative Commons licence and your intended use is not permitted by statutory regulation or exceeds the permitted use, you will need to obtain permission directly from the copyright holder. To view a copy of this licence, visit <http://creativecommons.org/licenses/by-nc-nd/4.0/>.

© The Author(s) 2025